Kinobead profiling reveals reprogramming of B-cell receptor signaling in response to therapy within primary CLL cells.

Linley AJ[1], Griffin R[2], Cicconi S[2], D'Avola A[3$], MacEwan DJ[4], Pettit AR[1], Kalakonda N[1], Packham G[3], Prior IA[5], Slupsky JR[1].

1. Department of Molecular and Clinical Cancer Medicine, Institute of Translational Medicine, University of Liverpool, Sherrington Building, Ashton Street, Liverpool, UK.
2. CRUK Clinical Trials Unit, University of Liverpool, Waterhouse Building, Ashton Street, Liverpool.
3. Southampton Cancer Research UK Centre, Cancer Sciences Unit, Faculty of Medicine, University of Southampton, Southampton, UK.
4. Department of Molecular and Clinical Pharmacology, Institute of Translational Medicine, University of Liverpool, Sherrington Building, Ashton Street, Liverpool, UK.
5. Department of Cellular and Molecular Physiology, Institute of Translational Medicine, University of Liverpool, Nuffield Wing, Crown Street, Liverpool, UK.

[$] Current Address: The Francis Crick Institute, 1 Midland Road, London, UK.

Corresponding author: Dr Adam J Linley, Department of Molecular and Clinical Cancer Medicine, Institute of Translational Medicine, University of Liverpool, Sherrington Building, Ashton Street, Liverpool, UK; alinley@liverpool.ac.uk; +44(0)151 794 5310

Running head: *Therapy brings about BCR signal changes.*

Key points

1. **sIgM signaling patterns alter following in vivo therapy using either chemoimmunotherapy or ibrutinib.**

2. **Kinobeads provide a novel method for high-resolution investigation of signaling in primary CLL cells.**

Abstract

Induction of signaling via cell surface receptor activation is a critical driver of CLL pathobiology, especially via the B-cell receptor (BCR), which promotes tumor survival and progression. The vital nature of BCR signaling has been recognized through the development of kinase inhibitors (KI), most notably ibrutinib, that target key nodes within this pathway. Current efforts to monitor signaling investigate expression of a highly confined series of kinases and phosphoproteins. While generating key insights, full appreciation of their wider significance to malignant pathology and therapy response remains an unresolved issue. Here, we describe a kinobead-based protocol, used in conjunction with mass-spectrometry (MS) or immunoblotting, to study surface-IgM (sIgM) signaling within primary CLL cells. Employing this approach, we isolated a 'fingerprint' of over 30 kinases which displayed unique, patient-specific response to sIgM stimulation, and which displayed greater activation change in CLL cells from patients who had undergone prior chemoimmunotherapy (CIT) compared to those from untreated/treatment-naïve patients. Matched sample analysis of ARCTIC/AdMIRe clinical trial patients revealed the unique nature of the kinome response was present at the intra-patient level, while longitudinal profiling of IcICLLe trial patients supported this as well as showing our finding related to ibrutinib therapy. Refinement of the kinome fingerprint determined 4 kinases linked to proliferation found to be present to a significantly higher level within previously treated patient cells. Proliferation assays confirmed that these patients possess higher proliferative capacity, implying alterations of signaling resulting in promoting of biological processes critical to malignant cells. Collectively, these data represent the first comprehensive investigation into BCR signaling response within CLL, where our probing of kinase active sites reveals unique evidence of adaptive reprogramming in response to therapy.

Introduction

The accumulation and survival of chronic lymphocytic leukemia (CLL) cells is strikingly dependent on signaling from activated cell surface receptors.[1,2] This applies especially to the B-cell receptor (BCR) where antigen-dependent and –independent activity has been linked to disease development.[1,3-5] For example, retained anti-IgM signaling capacity is associated with progressive disease,[6] and kinase inhibitors (KI) targeted against BCR signaling pathways (especially the Bruton's tyrosine kinase (BTK) inhibitor ibrutinib) can induce impressive clinical responses in patients with CLL or some subtypes of non-Hodgkin's lymphoma.[7-9] In addition to disease pathogenesis, altered signaling influences response to therapy. This is clearest in the context of acquired resistance to ibrutinib which is commonly associated with mutations of BTK itself or one of its downstream effectors, phospholipase Cγ2 (PLCγ2), where mutations within either result in production of proteins which retain activity but bind ibrutinib less avidly, or are hyper-responsive to upstream activating pathways, respectively.[10,11]

Kinase activation and inhibition in primary CLL cells has generally been analyzed by examining kinase-substrate phosphorylation using phospho-specific antibodies to identify modified amino-acids. While such an approach can provide important insight, interpretation of results can be challenging. For example, the activity of many kinases is influenced by multiple phosphorylation events which can be activating or inhibiting. Where phosphorylation at multiple sites on an individual kinase is detected, it can be

difficult to determine whether these are on the same molecule, or whether sub-populations of kinases with distinct patterns of phosphorylation (and hence activity) co-exist. Upstream kinase activity can be inferred from patterns of substrate phosphorylation, but redundancy amongst kinases (where several kinases may be able to modify an individual phospho-acceptor site) limits the utility of this approach. Finally, changes in phosphorylation will reflect changes not only in kinase activity, but also their counteracting phosphatases.

Kinobeads provide a powerful new tool to probe kinase function.[12-15] In this approach cell lysates are incubated with beads coated with broad-specificity type 1 KI, allowing binding of a large proportion of the expressed kinome. Bound kinases can then be profiled using mass-spectrometry (MS) or analyzed directly using immunoblotting. Kinobead-MS technology was initially deployed to determine the specificity profiles of KI, since binding of KI to target kinases prevents their subsequent capture by the kinobeads.[16] However, kinase capture can also be influenced by changes in the abundance of the kinases and, in particular, active site conformation. Many kinases exist in an auto-inhibited form and their activation requires conformational change. For example, BTK adopts multiple conformations allowing graded activation following cell stimulation,[17] and ERK activation requires a MEK-dependent switch to an active conformation.[18] Taking these considerations into account, kinobead technology has been used more recently to probe kinase activation in response to cell stimulation and, in particular, to reveal adaptive "rewiring" of kinase networks following exposure to KI that can lead to.[12,19]

Here, we have developed the kinobead approach for analysis of malignant B-cells and used it for the first time to characterize signaling in primary CLL. We show kinobeads can be used to assess active site occupancy by kinase inhibitors, including in ibrutinib-treated patients.

Materials and Methods

Cells

Primary cells from patients diagnosed with CLL according to iwCLL-2008 criteria were donated by patients attending clinics at Royal Liverpool and Broadgreen Hospitals NHS Trust following informed consent according to the Declaration of Helsinki. Samples were provided as heparinized whole blood from which peripheral blood mononuclear cells (PBMC) were isolated using Lymphoprep (Axis Shield, Oslo, Norway) and cryopreserved as previously described.[20] Alternatively, primary cells from patients recruited to the ARCTIC/AdMIRe (ISRCTN16544962)and IcICLLe (ISRCTN12695354)clinical trials were obtained from the UK CLL Clinical Trials BioBank (Liverpool, United Kingdom). In all cases, cells were recovered as outlined before,[20] counted and diluted to $1x10^7$/ml using pre-warmed complete medium (RPMI1640+Glutamax (Gibco) supplemented with 10% (v/v) fetal calf serum (FCS) and 1% (v/v) Pen/Strep). The B-CLL-derived cell line MEC-1 was cultured in complete medium. Cell line identity was confirmed using STR analysis (Powerplex 16 System, Promega) and absence of mycoplasma was confirmed using Mycoplasma PCR detection kit (Applied Biological Materials).

Characterization of primary CLL cells

Cells from non-trial patients underwent cell surface phenotyping using anti-CD19/APC, anti-CD5/PerCP Cy5.5 (both Biolegend, Cambridge, U.K.), anti-IgM/PE

(Dako, Ely, U.K.) and appropriate isotype control antibodies, and using an Attune NXT flow cytometer (Thermo Fisher Scientific, Loughborough, U.K.). Signaling capacity was determined by measuring the proportion of malignant cells that were able to flux intracellular calcium (iCa^{2+}) following treatment with $F(ab')_2$ anti-IgM, as described previously[21] using a FACS Calibur (BD Biosciences, Oxford, U.K.). All flow cytometry data was analyzed using FlowJo (TreeStar, Oregon, USA).

Treatments

Primary CLL samples were treated with 20 μg/ml anti-IgM or control $F(ab')_2$ (Southern Biotech, Cambridge Biosciences, U.K.) for 5 minutes at 37°C/5% CO_2. MEC-1 cells were pre-treated for 1 hour with 500nM ibrutinib or dasatinib prior to protein lysis.

Kinome analysis

Isolation and detection of kinase proteins was performed using a kinobead-based protocol similar to that described previously,[12], while kinase mRNA expression was screened using Nanostring. Detailed descriptions of kinome analysis are outlined in Supplementary Methods.

Measurement of stimulation induced proliferation of CLL cells.

Proliferation of primary CLL cells in response to stimulation was performed using a co-culture system using HS-5 bone marrow stromal cells. The day prior to beginning assays, HS-5 underwent irradiation using 3Gy for 25 minutes to inhibit stromal cell proliferation, however retaining their ability to support CLL cells. These were subsequently plated at 5 $x10^5$ cells/well and incubated at 37°C/5%CO_2 overnight. The following day, CLL cells were recovered as outlined above prior to labelling with Cell Trace CFSE (Thermo) in accordance with the manufacturer's protocol. Labelled CLL cells were subsequently plated onto HS-5 cells at 1 $x10^6$/well and incubated for 20 minutes prior to stimulation with 7.5μg/ml CpG-ODN-2006 or DMSO to represent unstimulated control. Co-cultures were incubated for 7 days, at which point CLL cells were carefully recovered, washed using flow buffer and then stained with anti-CD19/APC and anti-CD5/PerCP Cy5.5 for 15 minutes on ice in darkness. Cells were washed and resuspended in flow buffer before analysis using an Attune NXT flow cytometer. Population of decreasing CFSE staining, therefore showing proliferation of CLL cells were measured in live, singlet populations, gated on for dual expression of CD19 and CD5.

Immunoblotting

For direct analysis, cells were lysed using radioimmunoprecipitation assay (RIPA) buffer whereas for kinobead analysis, elutions from kinobeads were mixed with and equal volume of 2x loading buffer prior to SDS-PAGE. Immunoblotting was performed using anti-phospho-ERK-1/2 (Y202/T204), anti-ERK, anti-phospho-AKT (S473), anti-AKT, anti-phospho-SYK (Y525/526), anti-SYK, anti-BTK (Y223) or anti-BTK (all Cell Signaling Technologies, Hitchin, U.K.). Anti-actin (Sigma) or anti-HSC-70 (Insight Biotechnology) antibodies were used as loading controls. Bound primary antibodies were detected using species-specific fluorophore-conjugated secondary antibodies (LiCOR) and imaged using a LiCOR Odyssey CLx instrument, or HRP-conjugated secondary antibodies (Dako) with the ChemiDoc-It imaging system (BioRad) and VisionWorks software.

Data sharing
All kinases detected by Nanostring and kinobead-MS are listed in **Supplementary List 1** with the online version of this article. For data values, please contact alinley@liverpool.ac.uk.

RESULTS

Validation of kinobeads for the analysis of malignant B cells

We first examined the ability of kinobeads bearing different broad-specificity KI to capture kinases using the MEC-1 cell line. MEC-1 cells were derived from a CLL patient undergoing prolymphocytoid transformation[22] and were selected because they have readily detectable levels of constitutively active kinases, including ERK1/2 and AKT (**Supplemental Figure 1A**). A schematic workflow for a typical experiment is shown in **Figure 1A**. Three separate experiments were performed.

We found that the most effective kinobeads for kinase capture were those bearing Ki-NET (CTx-0294885). These isolated up to 132 kinases in total (i.e., identified in at least one of the experiments performed), with a core set of 107 kinases being detected in all three experiments (**Figure 1B, C**). Captured kinases included representatives from all kinase sub-families and well-characterized BCR signalosome components, including LYN, SYK and BTK (**Figure 1C**). By contrast, kinobeads bearing bisindolylmaleimide-X (Bis-X), dianillopyrimidine, purvalanol-B, pp58 or VI16832 captured substantially fewer kinases (**Figure 1B**). Each kinobead also captured various non-kinases and, in some instances, the number of non-kinase targets captured substantially outweighed the number of kinases (e.g. purvalanol-B). Identified non-kinases may reflect direct capture of non-kinase targets or indirect capture of kinase-associated proteins. Importantly, ~70% of the unique kinases identified using any of the 6 kinobeads were captured using Ki-NET only (**Supplementary Figure 1B**) and we therefore focused on Ki-NET kinobeads for further studies.

We used Ki-NET kinobeads to investigate the effects of two tyrosine KI on the core set of 107 kinases captured from MEC-1 cells (**Figure 1C**). Ibrutinib and dasatinib are considered primarily as inhibitors of BTK and ABL, respectively, although both drugs have numerous additional kinase targets, some of which are shared.[23] Analysis was performed after 60 minutes of drug exposure; a time point at which we would not expect to observe substantial changes in the steady state expression of kinases. Thus, changes in kinase capture are likely to reflect both direct target engagement (thereby blocking kinobead binding) and secondary effects on downstream kinases.

The most striking effects of ibrutinib and dasatinib on kinase capture were observed within the TK and TK-like (TKL) families and appeared to be due to occupancy of direct targets (**Figure 1C**). Thus, BTK capture was reduced by >99% in cells treated with ibrutinib (**Figure 1C, D**). BTK capture was also essentially ablated in cells exposed to dasatinib **(Figure 1C)**, which is also known to inhibit BTK.[24] Other kinases with substantially reduced capture in drug treated cells included LCK, FYN, LYN, FGR, SRC, CSK, TEC, BLK and RIPK2, which are all known to be directly inhibited by both ibrutinib and dasatinib.[23,25,26]

We also observed more modest reductions in capture of a number of other kinases including ERK1 and 2, PKCβ and IKKβ **(Figure 1D)** which are not known as direct targets of ibrutinib/dasatinib but are likely to be modulated as a response to upstream effects. Reduced capture of MEK1 and MEK2 was consistent with the observed reduction of phosphorylation of the MEK1/2 substrates ERK1/2 detected by immunoblotting (**Supplementary Figure 1**). Thus, kinobeads reveal both the direct occupancy of kinase active site by drug, as well as indirect modulation of active site availability of non-target kinases.

Kinobead analysis of primary CLL cells

Having validated our approach to profile the kinome of B-cells, we next performed Ki-NET kinobead analysis of primary samples from a cohort of 32 CLL patients. Profiling was performed using cells treated either with control antibody or with anti-IgM to allow us comparison between the "basal" kinobead signature in the absence of exogenous stimulation and that in response to sIgM stimulation respectively. Analysis was performed at 5 minutes following addition of anti-IgM (or control antibody) since previous analyses showed that this was suitable time point for analysis of both proximal (e.g. LYN, SYK) and distal (e.g. ERK1/2) signaling responses in CLL cells. To avoid artefacts associated with extended cell manipulations we did not purify malignant cells before stimulation/analysis. In all cases, cell viability was ≥90%. In the first instance, we sought to determine if the kinome fingerprint discovered with MEC-1 the existence of could be replicated in primary CLL B-cells. Through this, we were able to recognize a signature of 104 kinases captured by the Ki-NET beads in both control and IgM-stimulated. As expected, there was considerable overlap between the kinases captured from MEC-1 and primary cells. For example, 74% of these 104 kinases were also detected in the MEC-1 cells.

To further probe the performance of kinobead analysis, we compared the spectrum of kinases identified using kinobeads with expression of the kinome at the RNA level detected using nCounter XT HuV2 Kinase arrays (Nanostring). RNA analysis detected 397 of the 535 possible kinases and pseudokinases coded by the human genome (**Supplementary Figure 2A**). Coverage of the major kinase subfamilies was largely similar between analytical techniques and kinobeads appeared to be able to capture kinases over a wide expression range, at least as determined by RNA analysis.

Although capture of some kinases was relatively consistent across all samples, others were more variably detected. As such, it was possible to determine a wider signature of 104 kinases within at least 50% of the cohort, while a more refined, core fingerprint of 37 kinases was recognized across at least 75% of patients. To the best of our knowledge, this represents the most comprehensive signaling profile of primary CLL cells. Consistent with the known heterogeneity of sIgM signaling capacity in CLL cells,[3,27] with substantial variation in the response to anti-IgM between samples analyzed using kinobeads (**Figure 2**). Some samples showed relatively few changes in kinase capture following anti-IgM-stimulation, whereas others showed strong increases in capture of a relatively large proportion of the detected kinome. Visual examination recognized how each patient demonstrated a unique fingerprint, thus suggesting each patient generated a unique signaling response across the wider kinome in response to sIgM activation. Initially these fingerprints were stratified accordingly based on signaling and prognostic indicators (*IGHV* mutation status, Ca^{2+}

flux, sIgM expression, Binet staging and karyotype), which indicated little correlation (**Figure 2A**). However, deeper analysis of patient characteristics indicated that induced kinobead fingerprints appeared to correlate most strongly with treatment status in that patients who had previously received CIT (previously treated/PT) exhibited greater changes in kinase capture compared to treatment naïve (TN) patients (**Figure 2B**). Comparison of this fingerprint at basal level (+Control F(ab')2) along with their mRNA expression found a highly significant level of correlation (P=<0.0001; **Supplementary Figure 2B**). This suggested that difference in kinases between TN and PT patients was solely the result of sIgM engagement. To determine if alterations of the kinome resulted from changes in phosphatase activity, we examined the expression of key examples reported in B-cells,[28-35] comparing both TN and PT patients. These were unable to recognize differences in phosphatase activity between these patient groups (**Supplementary Figure 3**).

Although there is known redundancy for certain kinases and others are known to be utilized by different signal networks, the numbers recognized as part of the wider and core kinome fingerprints suggested potential for multiple pathways being recruited in response to activation of sIgM. To assess this, we focused on the core signature and used STRING analysis to determine which KEGG pathways each kinase was associated with using a strict false discovery rate (FDR) (<0.0001). Based on this, we identified 20 KEGG pathways associated with this kinome fingerprint (**Figure 2C**) highlighting the shared roles/function kinases. Some of these pathways have been previously associated with CLL cell signaling, most obviously BCR, but also Chemokine, MAPK, mTOR, TLR PI3K and NFκB. Others however, such as FoxO, RAS, cAMP, WNT, and HIPPO have been less focused upon. Based on the data described above, this suggested the potential of a CIT to influence multiple different pathways recruited following sIgM activation. To emphasize this, the core kinome fingerprint was organized to compare the average relative change in kinase binding to Ki-NET beads in TN and PT patients and using a cut-off of <1 fold change (Log2) upon sIgM activation (**Figure 2D**), we identified NDR1 (STK38), PKN1, CAM2KG, PHKG2, JNK1 (MAPK8), HCK, FYN, JAK1 and CSK as kinases with the greatest relative change in response to sIgM activation. Based on our analysis, these kinases are accumulatively involved in 13 KEGG pathways.

Detection of intra-patient kinome signaling heterogeneity influenced by therapy.

Chemoimmunotherapy

To further investigate the role of therapy on sIgM-induced signaling, we next performed matched sampled analysis. In the first instance, this involved patients (n=10) who had been recruited to the ARCTIC/AdMIRe clinical trials. Samples taken from these patients at disease progression (DP) and thus following receipt of FCR-based treatment, had been used as part of the original patient cohort. To investigate changes in these patients, kinobead-MS was carried out on the baseline (BL) samples for these patients and subsequently compared to the DP fingerprints (**Figure 3**). In terms of the BL samples, heterogeneity of responses was again evident meaning prominent intra-patient variability kinome signaling responses in addition to the inter-patient variability of recognized in the main cohort. This implied that sIgM signaling responses were unique not just in terms of patients but also related to time and consequence of treatment. Intriguingly, it was possible to segregate these 10 patients based on their DP kinome fingerprints to determine 2 main responses

(**Figure 3A**). These were 'Low Response/LR' patients which largely demonstrated reduced binding to Ki-NET beads across the entire fingerprint (Average= -0.34; Log2 fold change) and 'High Response/HR' which demonstrated increased kinase binding. For HR patients, there a 1.4-fold change (Log2) across the whole fingerprint and 12 (33%) where relative binding was greater than 1, as according to our previous cut off (**Figure 3B**). From our STRING analysis, we found 17 of the kinases within our core fingerprint have been shown to interact with each other with experiment evidence. We therefore used this to create a signaling atlas of these 17 kinases to illustrate kinome activation change between LR and HR patients (**Figure 3C**).

Ibrutinib

Small molecule agents have become increasingly prevalent as therapy options for CLL, the most evident example of this being ibrutinib. We next sought to investigate if the findings for CIT could be repeated the actions of this agent, for which we examined samples donated by patients recruited to the IcICLLe clinical trial. As with the ARCTIC/AdMIRe patients, a selection of these (n=8) had undergone profiling as part of the original cohort. Longitudinal profiling was carried out on 4 of these, comparing their BL, pre-ibrutinib sample, to those taken 1- and 6 months following initiation of ibrutinib (**Figure 4**). While core fingerprints for these patients had demonstrated considerable heterogeneity at baseline, our data found that 1 month following initiation of ibrutinib therapy, there was a marked increased kinase binding in 3/4 patients (**Figure 4A**). All patients showed a loss of binding of BTK, illustrating how the in vivo action of ibrutinib and occupation of its active site resulted in a filaiure to interact with Ki-NET beads. Moreover, there was an inability to isolate BLK, which shows significant homology to BTK, which was in agreement with experiments performed using MEC-1 cells. Kinobead-MS was able to demonstrate continued inhibition of BTK in samples taken 6 months following initiation of ibrutinib loss of Ki-NET isolation. Interestingly, 2 of the 3 patients who had shown increased signaling at 1 month appeared to experience resolution, while the remaining patient appeared to show increased kinomic signaling (**Figure 4A**). In a similar manner to our CIT trial comparison, it was possible to determine the biggest average changes in kinase binding over the 3 timepoints (**Figure 4B**), which allowed the assembly of an ibrutinib kinome signaling atlas comparing averaged responses at each timepoint (**Figure 4C**).

Cell from PT CLL patients show increased proliferative capacity

Up to this point, our data had illustrated the ability of sIgM activation to involve multiple signaling pathways and how this could be influenced by therapy. The possible consequence of this adaptation is that behavior of tumour B-cells could be altered by therapy. To that end, we finally sought to determine if kinobead-MS could be employed to identify nodes associated with critical aspects of malignant biology (**Figure 5**). To do this, we employed a biostatisical approach to refine the core fingerprint derived from our original patient cohort, which identified 14 kinases for further analysis. Interestingly, STRING analysis found that 10 of these (71%) have been shown to interact with one another with experimental evidence (**Figure 5A**), suggesting the presence of a signaling nexus associated with treatment in primary CLL cells. Interquartile range (IQR) comparison identified 4 of these (SYK, FAK2, GAK and RSK2 as demonstrating significant differences between TN and PT patients (**Figure 5B**). SYK is a recognized driver of proliferation in CLL,[36,37] while the other kinases have described roles in other tumour, [38-41] however not in the setting of CLL.

Thus, we sought to examine if PT patients demonstrated increased proliferation following BCR stimulation.

To do this, we used CFSE proliferation assays to examine CLL cell proliferative response 7 days following stimulation with CpG-ODN (**Figure 5C**). This found that cells from PT patient were able to undergo markedly increased levels of proliferation in response to CpG treatment compared to TN patients (**Figure 5C**), appearing to confirm our hypothesis. underwent noticeably more rounds of replication compared to TN.

DISCUSSION

In the current study we employed a kinobead-based approach to illustrate the impact of therapy on sIgM signaling within CLL cells. This impact was observed in cells from patients who had received traditional CIT as well as in cells from patients following treatment with ibrutinib. In the former, prior CIT treatment was associated with increased ability of kinobeads to capture kinases in IgM-stimulated cells. In the latter, we observed that ibrutinib treatment inhibited the ability of the kinobeads to capture BTK regardless of whether the cells were incubated with control Ig or with anti-IgM. However, with the latter, our approach was able to recognize increased signaling in

The most common method for investigating signaling in CLL involves the use of antibodies to screen restricted numbers of kinases and phosphoprotein targets using immunoblotting or flow cytometry. While informative, these methods lack the resolution required to observe widespread changes to signaling mediators within cells in response to various conditions. Alternatively, MS is an emerging technology, in terms of CLL, used so far to investigate malignant biology and severity.[42-44] Although this has provided a global view of protein expression in CLL cells, it has not been useful to understand signaling changes, either in response to receptor activation, or following receipt of therapy. In our approach we combined MS with a kinobead-based protocol to examine changes to signaling in CLL cells following sIgM activation. This method reproducibly isolated over 100 kinases from MEC-1 and primary CLL cells as detected by MS, with good coverage of all major kinase subfamilies. Comparison with mRNA expression of the kinome showed that kinobeads isolated approximately a quarter of all kinase proteins potentially expressed in CLL cells, where ability to capture individual kinases for protein identification by MS was not related to mRNA expression levels of that kinase. The reasons why we were unable to detect the full kinome expressed by CLL cells is unclear but could reflect either lack of translation of detected mRNA to protein, absence of kinase active site availability (e.g. through autoinhibition), or to the affinity of the expressed kinases for the kinobeads we used. These latter two possibilities explain why we were only able to isolate and detect one member (RIOK2) of the atypical kinase subfamily by kinobeads. Nevertheless, consistent with studies on other cell types,[12-15] our results show that kinobeads were able to detect a substantial proportion of the kinome in malignant B-cells.

Kinobeads were originally deployed to probe the selectivity of KI[16] where the strongest changes in capture are due to direct occupancy of kinase active sites. Our data is in agreement with this, and we found that treatment of MEC-1 cells with ibrutinib or dasatinib resulted in reductions of known targets for these agents such as BTK and BLK for ibrutinib, and LYN and FYN for dasatinib. Importantly, ibrutinib covalently modifies BTK at Cys[481] and is therefore irreversibly bound to this protein. When used

to analyze drug occupancy in CLL cells from patients receiving ibrutinib therapy, kinobeads demonstrated targeting of BTK. As far as we are aware, this is the first time kinobeads have been used to directly demonstrate target-drug interactions in an *in vivo* situation. Thus, kinobeads could be used to monitor target occupancy in individual patients to personalize dosing regimens.

In addition to loss of capture of known ibrutinib/dasatinib targets in MEC-1 cells, we also observed both reductions and increases in capture of non-target kinases. Reduced capture of non-target kinases likely reflects signaling pathway cross-talk where direct inhibition of upstream kinases leads to reduced activity of interlinked kinases. For example, we demonstrated by MS that ibrutinib treatment of MEC-1 cells reduced activity of MEK1/2, which can be activated downstream of BTK.[45] We subsequently confirmed this finding by immunoblotting, showing that ibrutinib treatment reduces phosphorylation of the MEK1/2 substrates ERK1/2. Interestingly, we also detected a small number of kinases with increased kinobead capture in ibrutinib/dasatinib-treated cells. Increased capture may reflect relief of inhibition by upstream kinases in drug treated cells, or an indirect adaptive cell response. For example, kinobead analysis of MEK inhibitor (AZD6244)-treated triple negative breast cancer cells demonstrated adaptive activation of receptor tyrosine kinases where additional treatment with the proteasome using bortezomib was required to halt the adaptive reprogramming response.[12] Future studies will focus on the biological significance of this potential rewiring revealed by kinobead analysis of malignant B-cells to determine whether targeted inhibition of these kinases with increased binding may be an effective strategy to increase the therapeutic activity of drugs such as ibrutinib.

We extended our analysis to profile anti-IgM signaling responses in primary CLL. As with MEC-1, it was possible to detect over 100 kinases, although this was not shared across the entire cohort, where it was possible to recognize a more consistent fingerprint of almost 40 kinases. In either instance this, to the best of our knowledge, represents the most comprehensive profiling of signaling mediators in primary CLL cells. It was interesting to note that individual samples varied widely in their response, and that samples from patients, with each member of our cohort demonstrating a unique kinomic signaling response. Signaling heterogeneity is a widely acknowledged phenomenon associated CLL. Generally, this is thought to result from using primary patient material. The unique nature of each patient's response, in addition to the resolution provided by kinobead-MS, revealed a complexity of sIgM signaling that has not yet been appreciated. Moreover, based on the extent of the kinome fingerprint isolated from patients, our data was able to illustrate the range of different signaling pathways recruited following engagement of this receptor. While some of these are recognised as being associated with BCR signaling in CLL, some are less well known. This means there appears to more breadth and complexity of signaling involved and implies that activation of the BCR essentially induces the recruitment of multiple signaling pathways into a network designed to promote a biological endpoint.

The anti-IgM-induced kinome signature did not correlate closely with signaling capacity measured using iCa^{2+} flux or sIgM expression which have been used widely in previous studies as a read-out of signaling. In some cases, kinobeads revealed widespread changes in kinase capture. Additionally, we could find little correlation with prognostic factors such as stage or karyotype. Our discovery of a potential link with increased signaling associated with receipt of therapy is intriguing. This was noticeable not only between patients but within individuals receiving CIT or ibrutinib

too as was the unique nature of the kinome response. Adaptation to signaling has been highlighted previously, primarily with small molecule agents.[46,47] However, it has not yet been described for CLL and little has been done to explore the potential influence of CIT on the wider BCR signaling response.

One possible explanation for such a broad effect was reduced phosphatase activity, which could influence a large number of kinases. However, we were unable to identify a clear relationship between expression of a panel of phosphatases/inhibitory receptors and treatment status to support this concept. Many kinases depend on heat shock proteins (HSP) to maintain their active confirmation and treatment with the HSP-90 inhibitors AUY922 and PU-H71 is known to alter HSP expression and influence kinase expression.[48,49] Future experiments will investigate whether treatment associated changes in heat shock protein expression might provide an alternate explanation for the broad changes in kinase activation observed in some samples in our kinobead analysis.

Treatment with KI is becoming ever more prevalent to target cancer. This is especially evident with ibrutinib, which has proven to be a highly effective agent for the treatment of B-cell tumors including CLL. Although resistance to this agent has emerged, its overwhelming beneficial impact in terms of survival when compared to CIT[50] means it is likely to become front-line for patients. Our data highlight the ability of patients receiving CIT to experience changes to the kinome response, which has implications for their disease course. In particular, this could influence their response to ibrutinib. As shown by our data involving IcICLLe trial patients, some of whom had relapsed by to recruitment, prior receipt of CIT prior to receiving ibrutinib did not inhibit the in vivo action of the agent. However, we were not able to determine the clinical response of these specific patients had. Future work would involve examining the potential for CIT-induced signaling changes to possibly influence efficacy of ibrutinib. Rewiring of signaling needs to be recognized as a potential major issue to patients. Therefore, it is necessary to design rational therapy combinations, either multiple KI, or inclusion of other treatments in a manner that best suits the patient receiving it. We propose these findings act as basis to drive for personalized medicine or at very least signal-omics approach to investigating effects of therapy in CLL.

Acknowledgments

The authors would like to gratefully thank Drs Melanie Oates, Alix Bee, and Jessica Bithell (Molecular and Clinical Cancer Medicine, University of Liverpool) for providing clinical information and aiding in sample retrieval. In addition, we would like to thank Drs Cleidiane Zampronio and Juan Hernandez-Fernaud of the WPH Proteomics Facility (University of Warwick) for performing MS sample analysis and Drs Lucille Rainbow and Pia Koldkjaer of the Centre for Genomic Research (CGR) University of Liverpool for their assistance in Nanostring analysis. Finally, we would like to humbly thank the patients who provided samples for the work performed in this study. Funding for this work was kindly provided by the North West Cancer Research Fund (NWCR) (Grant ID:CR1041), Cancer Research UK (CRUK) (Grant ID C2750/A23669) and the Leuka John Goldman Fellowship for Future Science (Grant ID:153896).

Authorship

AJL optimized, designed and performed experiments, analyzed data, wrote, reviewed edited the manuscript and obtained funding. RG and SC carried out biostatisitical analysis of proteomic data. AD performed experiments and interpreted data. NK and ARP supplied clinical samples/input and reviewed the manuscript. DJM designed experiments and reviewed manuscript and obtained funding. GP, IAP and JRS designed experiments, interpreted data, reviewed and edited the manuscript and obtained funding.

The authors have no conflicts of interest to declare.

References:

1. Kipps TJ, Stevenson FK, Wu CJ, et al. Chronic lymphocytic leukaemia. *Nat Rev Dis Primers*. 2017; 19(3).
2. Burger JA, Wiestner A. Targeting B cell receptor signaling in cancer: preclinical and clinical advances. *Nat Rev Cancer*. 2018; 18(3):148-67.
3. Stevenson FK, Krysov S, Davies AJ, Steele AJ, Packham G. B-cell receptor signaling in chronic lymphocytic leukemia. *Blood*. 2011; 118(16):4313-20.
4. Dühren-von Minden M, Übelhart R, Schneider D, et al. Chronic lymphocytic leukaemia is driven by antigen-independent cell-autonomous signaling. *Nature*. 2012; 489(7415):309-12.
5. Minici C, Gounari M, Übelhart R et al. Distinct homotypic B-cell receptor interactions shape the outcome of chronic lymphocytic leukaemia. *Nat Commun*. 2017; 8: 15746.
6. D'Avola A, Drennan S, Tracy I, et al. Surface IgM expression and function are associated with clinical behavior, genetic abnormalities, and DNA methylation in CLL. *Blood*. 2016; 128(6):816-26.
7. Alinari L, Quinion C, Blum KA. Bruton's tyrosine kinase inhibitors in B-cell non-Hodgkin's lymphomas. *Clin Pharmacol Ther*. 2015; 97(5):467-77.
8. Byrd JC, Furman RR, Coutre SE, et al. Three-year follow up of treatment-naïve and previously treated patients with CLL and SLL receiving single agent ibrutinib. *Blood*. 2015; 125(16): 2497-506.
9. O'Brien S, Jones JA, Coutre SE et al. Ibrutinib for patients with relapsed or refractory chronic lymphocytic leukaemia with 17p deletion (RESONATE-17): a phase 2, open-label, multicentre study. *Lancet Oncol*. 2016; 17(1):1409-18.
10. Furman RR, Cheng S, Lu P, et al. Ibrutinib resistance in chronic lymphocytic leukemia. *N Engl J Med*. 2014; 370(24): 2352-4.
11. Woyach JA, Furman RR, Liu TM, et al. Resistance mechanisms for the Bruton's tyrosine kinase inhibitor ibrutinib. *N Engl J Med*. 2014; 370(24):2286-94.
12. Duncan JS, Whittle MC, Nakamura K, et al. Dynamic reprogramming of the kinome in response to targeted MEK inhibition in triple-negative breast cancer. *Cell*. 2012; 149(2):307-21.
13. Kurimchak AM, Shelton C, Duncan JE, et al. Resistance to BET bromodomain inhibitors is mediated by kinome reprogramming in ovarian cancer. *Cell Rep*. 2016; 16(5):1273-86.
14. Mundt F, Rajput S, Li S, et al. Mass-spectrometry-based proteomics reveals potential roles of NEK9 and MAP2K4 in resistance to PI3K inhibition in triple-negative breast cancers. *Cancer Res*. 2018; 78(10):2732-46.

15. Palve V, Kuenzi BM, Rix U. Unraveling the rewired network. *Nat Chem Biol*. 2018; 14(8): 746-7.
16. Bantscheff M, Eberhard D, Abraham Y, et al. Quantitative chemical proteomics reveals mechanisms of action of clinical ABL kinase inhibitors. *Nat Biotechnol*. 2007; 25(9): 1035-44.
17. Joseph RE, Wales TE, Fulton DB, Engen JR, Andreotti AH. Achieving a graded immune response: BTK adopts a range of active/inactive conformations dictated by multiple interdomain contacts. *Structure*. 2017; 25(10): 1481-94.
18. Zhang F, Strand A, Robbins D, Cobb MH, Goldsmith EJ. Atomic structure of the MAP kinase ERK2 at 2.3 A resolution. *Nature*. 1994; 367(6465):704-11.
19. Donnella HJ, Webber JT, Levin RS, et al. Kinome rewiring reveals AURKA limits PI3K-pathway inhibitor efficacy in breast cancer. *Nat Chem Biol*. 2018; 14(8): 768-77.
20. Krysov S, Dias S, Paterson A, et al. Surface IgM stimulation induces MEK1/2-dependent MYC expression in chronic lymphocytic leukemia. *Blood*. 2012; 119(1):170-9.
21. Mockridge CI, Potter KN, Wheatley I, Neville LA, Packham G, Stevenson FK. Reversible anergy of sIgM-mediated signaling in the two subsets of CLL defined by VH-gene mutational status. *Blood*. 2007; 109(10):4424-31.
22. Stacchini A, Aragno M, Vallario A et al. MEC1 and MEC2: two new cell lines derived from B-chronic lymphocytic leukaemia in prolymphocytoid transformation. *Leuk Res*. 1999; 23(2):127-36.
23. Wilson LJ, Linley A, Hammond DE, et al. New perspectives, opportunities, and challenges in exploring the human protein kinome. *Cancer Res*. 2018; 78(1):15-29.
24. Hantshel O, Rix U, Schmidt U, et al. The Btk tyrosine kinase is a major target of the Bcr-Abl inhibitor dasatinib. *Proc Natl Acad Sci USA*. 2007; 104(33): 13283-8.
25. Kim E, Hurtz C, Koehrer S, et al. Ibrutinib inhibits pre-BCR$^+$ B-cell acute lymphoblastic leukemia progression by targeting BTK and BLK. *Blood*. 2017; 129(9): 1155-65.
26. Chen J, Kinoshita T, Gururaja T, et al. The effects of Bruton's tyrosine kinase (BTK) inhibitors on collagen-induced platelet aggregation, BTK, and tyrosine kinase expressed in hepatocellular carcinoma (TEC). *Eur J Haematol*. 2018; doi: 10.1111/ejh.13148.
27. Packham G, Stevenson F. The role of the B-cell receptor in the pathogenesis of chronic lymphocytic leukaemia. *Semin Cancer Biol*. 2010; 20(6): 391-9.
28. Gabelloni ML, Borge M, Galletti J, et al. SHIP-1 protein level and phosphorylation status differs between CLL cells segregated by ZAP-70 expression. *Br J Haematol*. 2008; 140(1): 117-9.
29. Tibaldi E, Brunati AM, Zonta F, et al. Lyn-mediated SHP-1 recruitment to CD5 contributes to resistance to apoptosis of B-cell chronic lymphocytic leukemia cells. *Leukaemia*. 2011; 25(11): 1768-81.
30. Zhu JW, Brdicka T, Katsumoto TR, Lin J, Weiss A. Structurally distinct phosphatases CD45 and CD148 both regulate B cell and macrophage immunoreceptor signaling. *Immunity*. 2008; 28(2): 183-96.
31. Wu HJ, Bondada S. CD72, a coreceptor with both positive and negative effects on B lymphocyte development and function. *J Clin Immunol*. 2009; 29(1): 12-21.

32. Zikherman J, Doan K, Parameswaren R, Raschke W, Weiss A. Quantitative differences in CD45 expression unmask functions for CD45 in B-cell development, tolerance, and survival. *Proc Natl Acad Sci USA*. 2012; 109(1): E3-12.
33. Sieger N, Fleischer SJ, Mei HE et al. CD22 ligation inhibits downstream B cell receptor signaling and Ca(2+) flux upon activation. *Arthritis Rheum*. 2013; 65(3): 770-9.
34. Coughlin S, Noviski M, Mueller JL, et al. An extracatalytic function of CD45 in B cells is mediated by CD22. *Proc Natl Acad Sci USA*. 2015; 112(47): E6515-24.
35. Lumb S, Fleischer SJ, Weideman A, et al. Engagement of CD22 on B cells with the monoclonal antibody epratuzumab stimulates the phosphorylation of upstream inhibitory signals of the B cell receptor. *J Cell Commun Signal*. 2016; 10(2): 143-51.
36. Purroy N, Carabia J, Abrisqueta P, et al. Inhibition of BCR signaling using the Syk inhibitor TAK-659 prevents stroma-mediated signaling in chronic lymphocytic leukemia cells. *Oncotarget*. 2017; 8(1):742-56.
37. Slinger E, Thijssen R, Kater AP, Eldering E. Targeted antigen-independent proliferation in chronic lymphocytic leukemia through differential kinase inhibiton. *Leukemia*. 2017; 31(12):2601-7.
38. Susa M, Choy E, Liu X, et al. CyclinG-associated kinase is necessary for osteosarcoma cell proliferation and receptor trafficking. *Mol Cancer Ther*. 2010; 9(12):3342-50.
39. Sakurai MA, Ozaki Y, Okusaki D, et al. Gefitinib and luteolin cause growth arrest of human prostate cancer PC-3 cells via inhibition of G-associated kinase and induction of miR-630. *PLoS One*. 2014: 9(6): e100124.
40. Wu X, Zahari MS, Renuse S, et al. Phosphoproteomic analysis identifies focal adhesion kinase 2 (FAK2) as a potential therapeutic target for tamoxifen resistance in breast cancer. *Mol Cell Proteomics*. 2015; 14(11):2887-900.
41. Zhang X, Cai L, Zhao S, et al. CX-F9, a novel RSK2 inhibitor, suppresses cutaneous melanoma cells proliferation and metastasis through regulating autophagy. *Biochem Pharmacol*. 2019; 168: 14-25.
42. Kashuba E, Eagle GE, Bailey J, et al. Proteomic analysis of B-cell receptor signaling in chronic lymphocytic leukaemia reveals a possible role for kininogen. *J Proteomics*. 2013; 91: 478-85.
43. Eagle GE, Zhuang J, Jenkins RE, et al. Total proteome analysis identifies migration defects as a major pathogenic factor in immunoglobulin heavy chain variable region (IGHV)-unmutated chronic lymphocytic leukemia. *Mol Cell Proteomics*. 2015; 14(4): 933-45.
44. Johnston HE, Carter MJ, Larrayoz M, et al. Proteomics profiling of CLL versus healthy B-cells identifies putative therapeutic targets and a subtype-independent signature of spliceosome dysregulation. *Mol Cell Proteomics*. 2018; 17(4): 776-91.
45. Roskoski Jr R. Ibrutinib inhibition of Bruton protein-tyrosine kinase (BTK) in the treatment of B cell neoplasms. *Pharmacol Res*. 2016; 113(A): 395-408.
46. Johnson GL, Stuhlmiller TJ, Angus SP, Zawistowski JS, Graves LM. Molecular pathways: adaptive kinome reprogramming in response to targeted inhibition of the BRAF-MEK-ERK pathway in cancer. *Clin Cancer Res*. 2014; 20(10):2516-22.

47. Stuhlmiller TJ, Miller SM, Zawistowski JS, et al. Inhibition of lapatinib-induced kinome reprogramming in ERBB2-positive breast cancer by targeting BET family bromodomains. *Cell Rep*. 2015; 11(3): 390-404.
48. Jacobson C, Kopp N, Layer JV et al. HSP90 inhibition overcomes ibrutinib resistance in mantle cell lymphoma. *Blood*. 2016; 128(21): 2517-26.
49. Guo A, Lu P, Lee J, Zhen C, Chiosis G, Wang YL. HSP90 stabilizes B-cell receptor kinases in a multi-client interactome: PU-H71 induces CLL apoptosis in a cytoprotective environment. *Oncogene*. 2017; 36(24):3441-9.
50. Woyach JA, Ruppert AS, Heerema NA, et al. Ibrutinib alone or in combination with rituximab produces superior progression free survival (PFS) compared with bendamustine plus rituximab in untreated older patients with chronic lymphocytic leukemia (CLL): Results of Alliance North America Intergroup Study A041202. *Blood*. 2018; 132:6.

FIGURE LEGENDS

Figure 1: Kinobead analysis of MEC-1 cells. A; Schematic of the kinobead-MS used for this study. **B;** Pie graphs illustrating the numbers of kinase and non-kinase proteins isolated from MEC-1 cell lysates using 6 different kinobeads. **C;** MEC-1 cells were treated with ibrutinib or dasatinib (both at 500 nM) or left untreated as a control. After 60 minutes, cell lysates were prepared and kinase binding to Ki-NET beads was assessed using mass spectrometry. Kinases are grouped by subfamilies. Heat map shows mean change (log_2) in kinase binding for ibrutinib or dasatinib-treated cells relative to control cells for the core 107 kinases derived from three independent experiments. **D;** Graph showing results for ibrutinib for selected kinases, including direct targets (i.e., inhibited by ibrutinib in *in vitro* assays with IC_{50} <500 nM), kinases which are modulated by ibrutinib but are not direct targets, and kinases which are unaffected by ibrutinib. Graph shows mean (±error) binding normalized to control cells (set to 100%) with statistical significance of differences indicated (Student's t-test; *=P<0.05; **=P<0.01; ****=P<0.0001).

Figure 2: **Kinobead profiling of primary CLL cells**. Cell lysates were prepared from CLL samples (n=32) incubated with control antibody (no stimulation). Kinase binding was assessed using Ki-NET beads and mass spectrometry. **A;** Heatmaps showing signature of 37 kinases (fingerprint), showing relative changes in kinase binding (log2 fold change) in response to sIgM stimulation gained for each patient. Each patient (columns) was stratified according to different signaling and prognostic markers. **B;** Heatmap comparing kinome fingerprints for treatment naïve (TN) patients to previously treated (PT) patients within our cohort. **C;** Graph derived from STRING analysis of the kinome fingerprint, illustrating the KEGG pathways identified and the number of kinases from the fingerprint that are involved in each pathway. **D;** Graphs comparing average log2 fold changes for each node within the kinome fingerprint for TN and PT patients. Kinases with change >1 are highlighted with dots representing the different KEGG pathways they are linked to in order significance based upon their false discovery rate (FDR) (most significant to less significant).

Figure 3: Matched kinobead profiling of sIgM response in ARCTIC/AdMIRe patients. A; Heatmap comparing sIgM activation kinome fingerprints for ARCTIC/AdMIRe trial patients (n=10) using their baseline (pre-therapy) sample and their disease progression (DP) sample. For the latter, the heatmap is segregated based on each patient's response (based on log2 fold change)

into 'Low' (LR) and 'High' (HR). **B;** Graphs comparing average log2 fold changes for each node within the kinome fingerprint for LR and HR patients. **C;** Signaling atlas for 17 kinases known to interact (derived by STRING), illustrating the average changes in kinase binding upon activation of sIgM.

Figure 4: Longitundinal kinome analysis of the impact of ibrutinib on the sIgM response. A; Heatmap comparing sIgM activation kinome fingerprints for IcICLLe clinical trial patients (n=4) for baseline (pre-ibrutinib) sample to 1-month and 6-months following initiation of ibrutinib. **B;** Graphs comparing average log2 fold changes for each node within the kinome fingerprint at baseline, and subsequent time points following initiation of ibrutinib. **C;** Signaling atlas for the 17 interacting kinases within the core fingerprint illustrating the average changes in kinase binding upon activation of sIgM in relation to the receipt of ibrutinib.

Figure 5: Kinobead detection of kinases associated with increased proliferation in previously treated patients. **A;** Refinement of the core kinome fingerprint to 14 nodes and interaction of 9 of these based on STRING analysis. **B;** Interquartile range analysis of 4 of the refined signal fingerprints highlighting significant difference between TN and PT patients (*=P<0.05; **=P<0.01). **C;** Histograms showing CFSE proliferation of CLL cells in 2 representative patients highlighting increased proliferation in PT patients.

Supplementary Figure Legends

Supplementary Figure 1: **A**; Immunoblot analysis of MEC-1 cells showing expression of total and phospho-ERK-1/2 and AKT in control (NA), ibrutinib or dasatinib-pre-treated cells (both at 500 nM for 60 minutes). Actin was analyzed as an additional loading control. **B;** Venn diagrams showing overlap of kinases isolated by the different KI used to create kinobeads during this study.

Supplementary Figure 2: A; Graph comparing kinases identified at either mRNA level, protein (by kinobead isolation) or both in our patient cohort. **B;** Correlation of kinase mRNA expression determined by Nanostring between Treatment Naïve (TN) and Previously Treated (PT) patients.

Supplementary Figure 3: A; Flow cytometric analysis of inhibitory coreceptors and **B;** immunoblot analysis of phosphatases in three samples from untreated (UT) patients and three samples from previously treated (PT) patients. In **A**, graph shows results for individual samples and mean (±error). In **B**, GAPDH was analyzed as an additional loading control.

FIGURE 1

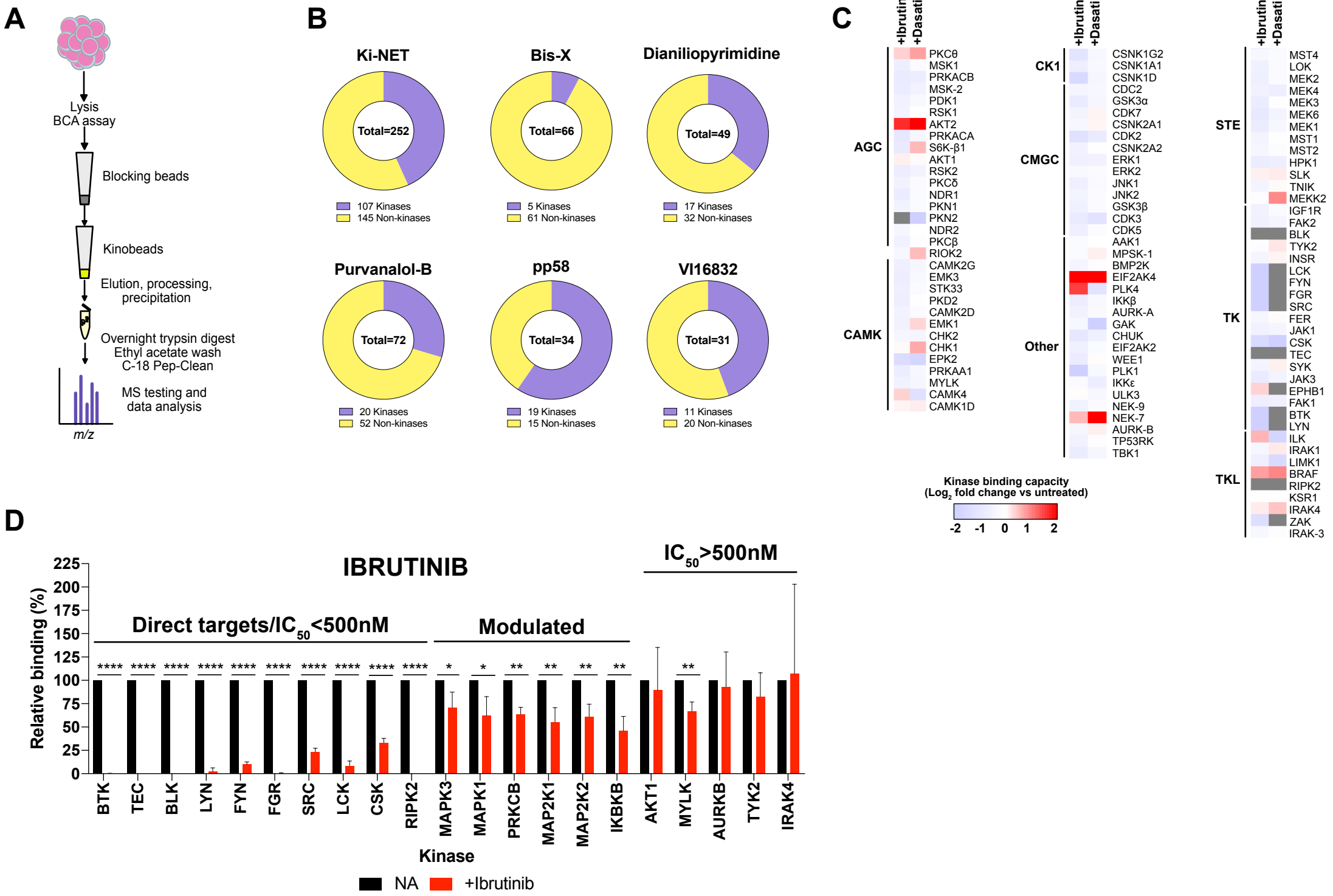
A
Lysis
BCA assay
Blocking beads
Kinobeads
Elution, processing, precipitation
Overnight trypsin digest
Ethyl acetate wash
C-18 Pep-Clean
MS testing and data analysis
m/z
B
Ki-NET
Total=252
107 Kinases
145 Non-kinases
Bis-X
Total=66
5 Kinases
61 Non-kinases
Dianiliopyrimidine
Total=49
17 Kinases
32 Non-kinases
Purvanalol-B
Total=72
20 Kinases
52 Non-kinases
pp58
Total=34
19 Kinases
15 Non-kinases
VI16832
Total=31
11 Kinases
20 Non-kinases
C
+Ibrutinib
+Dasatinib
AGC
PKCθ
MSK1
PRKACB
MSK-2
PDK1
RSK1
AKT2
PRKACA
S6K-β1
AKT1
RSK2
PKCδ
NDR1
PKN1
PKN2
NDR2
PKCβ
RIOK2
CAMK
CAMK2G
EMK3
STK33
PKD2
CAMK2D
EMK1
CHK2
CHK1
EPK2
PRKAA1
MYLK
CAMK4
CAMK1D
CK1
CSNK1G2
CSNK1A1
CSNK1D
CMGC
CDC2
GSK3α
CDK7
CSNK2A1
CDK2
CSNK2A2
ERK1
ERK2
JNK1
JNK2
GSK3β
CDK3
CDK5
Other
AAK1
MPSK-1
BMP2K
EIF2AK4
PLK4
IKKβ
AURK-A
GAK
CHUK
EIF2AK2
WEE1
PLK1
IKKε
ULK3
NEK-9
NEK-7
AURK-B
TP53RK
TBK1
STE
MST4
LOK
MEK2
MEK4
MEK3
MEK6
MEK1
MST1
MST2
HPK1
SLK
TNIK
MEKK2
TK
IGF1R
FAK2
BLK
TYK2
INSR
LCK
FYN
FGR
SRC
FER
JAK1
CSK
TEC
SYK
JAK3
EPHB1
FAK1
BTK
LYN
TKL
ILK
IRAK1
LIMK1
BRAF
RIPK2
KSR1
IRAK4
ZAK
IRAK-3
Kinase binding capacity
(Log2 fold change vs untreated)
-2 -1 0 1 2
D
IBRUTINIB
IC50>500nM
Direct targets/IC50<500nM
Modulated
Relative binding (%)
225
200
175
150
125
100
75
50
25
0
BTK
TEC
BLK
LYN
FYN
FGR
SRC
LCK
CSK
RIPK2
MAPK3
MAPK1
PRKCB
MAP2K1
MAP2K2
IKBKB
AKT1
MYLK
AURKB
TYK2
IRAK4
Kinase
NA
+Ibrutinib

FIGURE 2

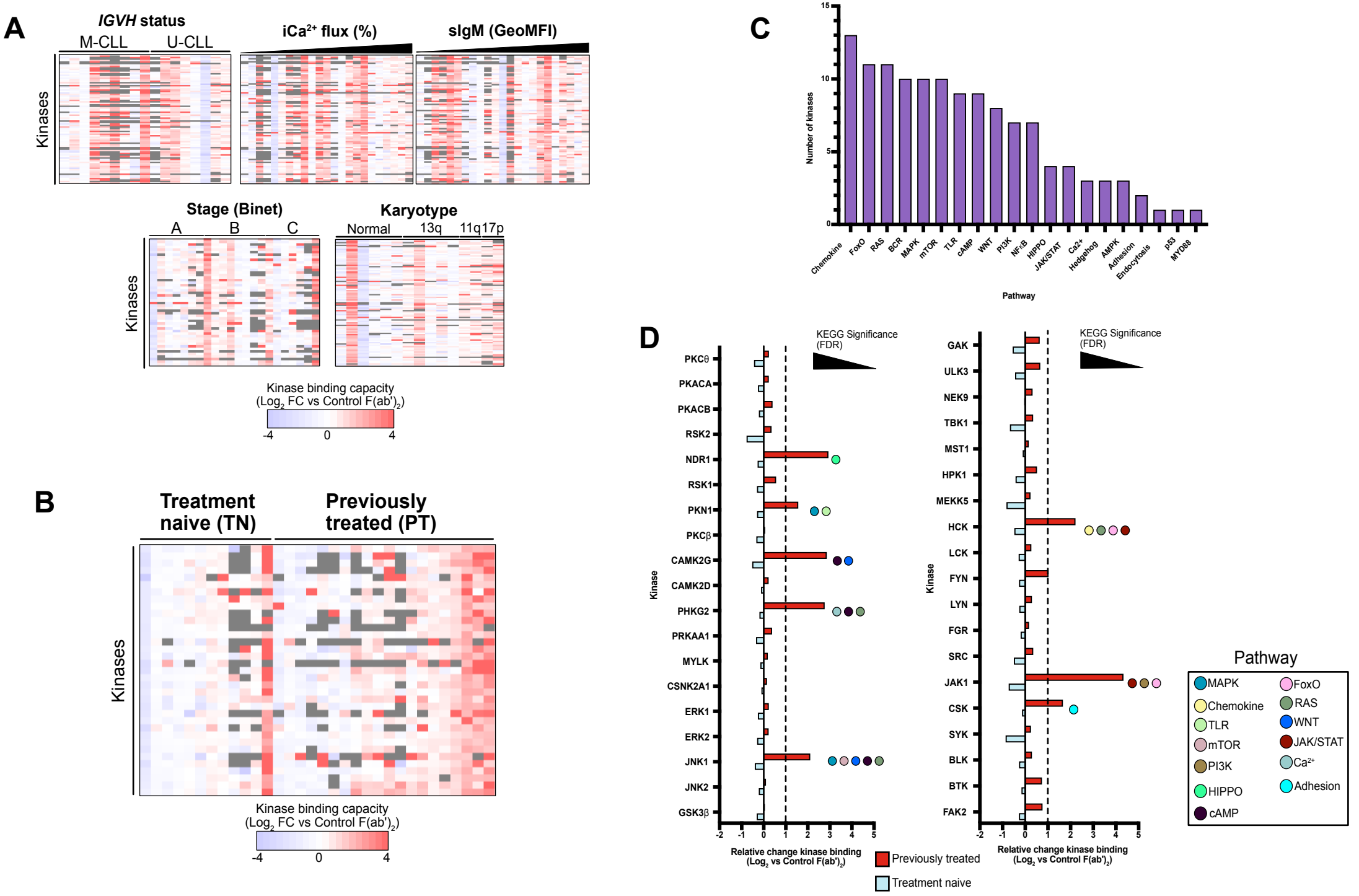
A
IGVH status
M-CLL
U-CLL
iCa2+ flux (%)
sIgM (GeoMFI)
Kinases
Stage (Binet)
A
B
C
Karyotype
Normal
13q
11q17p
Kinases
Kinase binding capacity
(Log2 FC vs Control F(ab')2)
-4
0
4
B
Treatment naive (TN)
Previously treated (PT)
Kinases
Kinase binding capacity
(Log2 FC vs Control F(ab')2)
-4
0
4
C
Number of kinases
15
10
5
0
Chemokine
FoxO
RAS
BCR
MAPK
mTOR
TLR
cAMP
WNT
PI3K
NFκB
HIPPO
JAK/STAT
Ca2+
Hedgehog
AMPK
Adhesion
Endocytosis
p53
MYD88
Pathway
D
KEGG Significance
(FDR)
PKCθ
PKACA
PKACB
RSK2
NDR1
RSK1
PKN1
PKCβ
CAMK2G
CAMK2D
PHKG2
PRKAA1
MYLK
CSNK2A1
ERK1
ERK2
JNK1
JNK2
GSK3β
Kinase
-2
-1
0
1
2
3
4
5
Relative change kinase binding
(Log2 vs Control F(ab')2)
KEGG Significance
(FDR)
GAK
ULK3
NEK9
TBK1
MST1
HPK1
MEKK5
HCK
LCK
FYN
LYN
FGR
SRC
JAK1
CSK
SYK
BLK
BTK
FAK2
Kinase
-2
-1
0
1
2
3
4
5
Relative change kinase binding
(Log2 vs Control F(ab')2)
Previously treated
Treatment naive
Pathway
MAPK
Chemokine
TLR
mTOR
PI3K
HIPPO
cAMP
FoxO
RAS
WNT
JAK/STAT
Ca2+
Adhesion

FIGURE 3

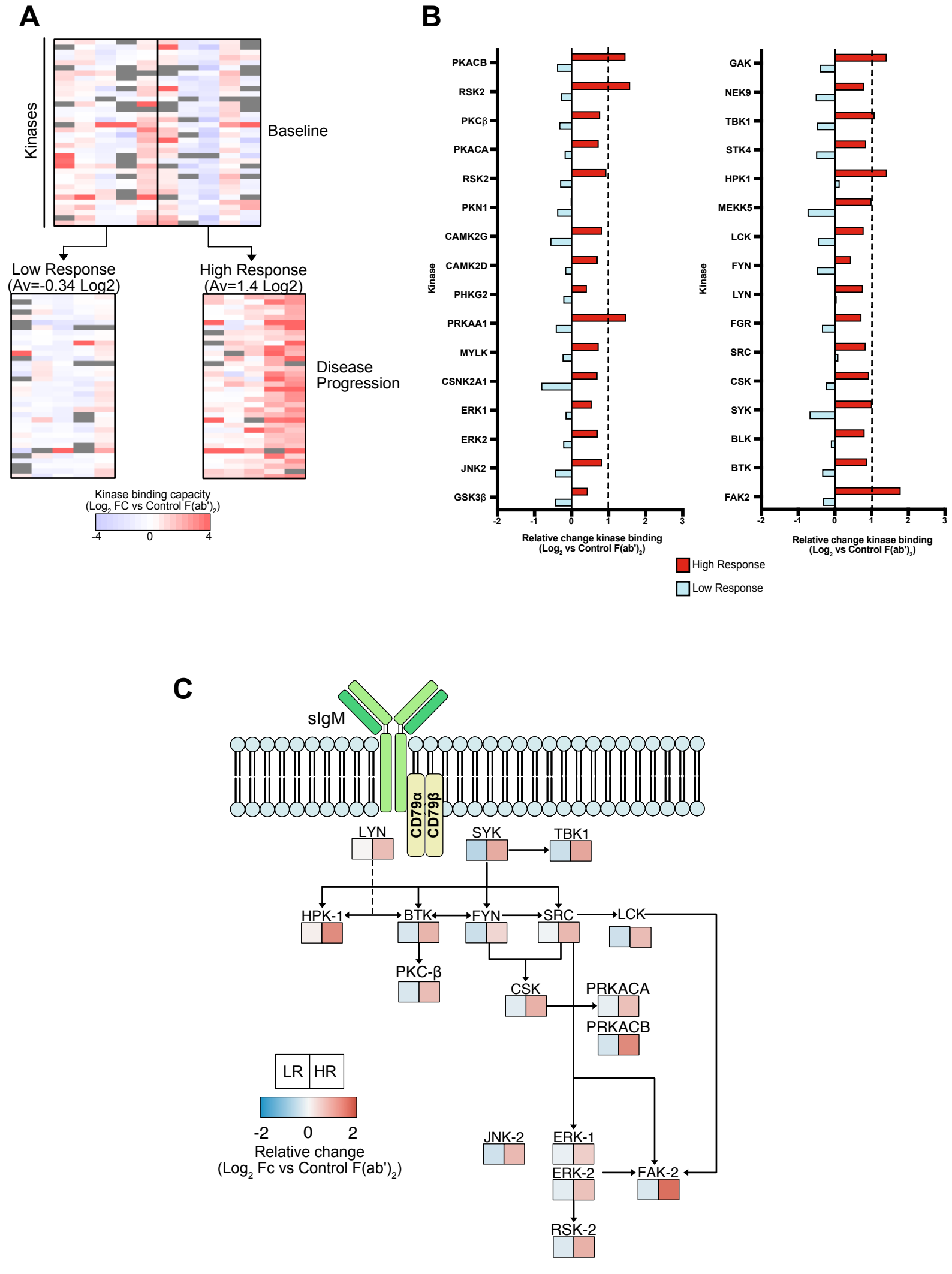

FIGURE 4

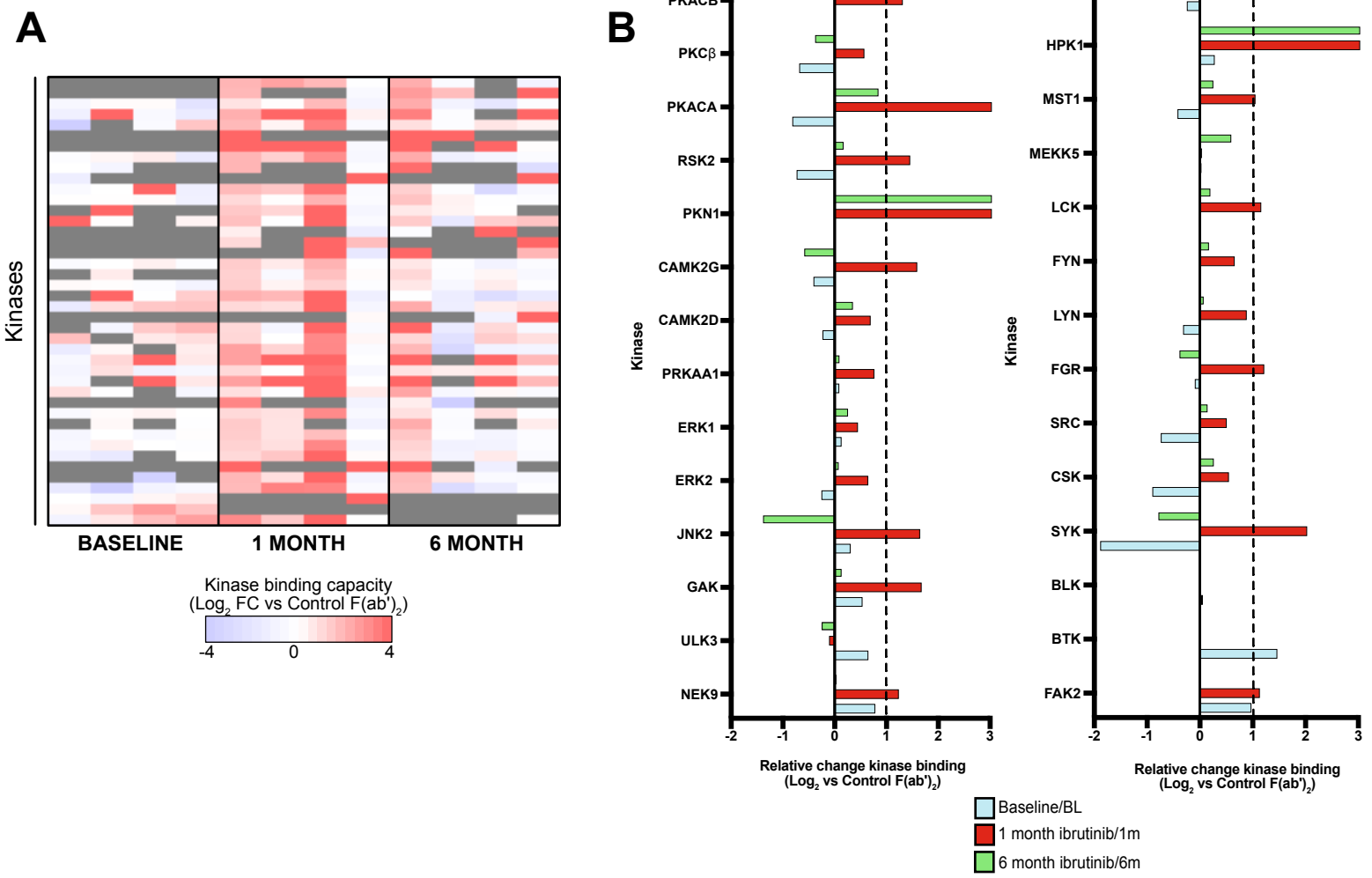

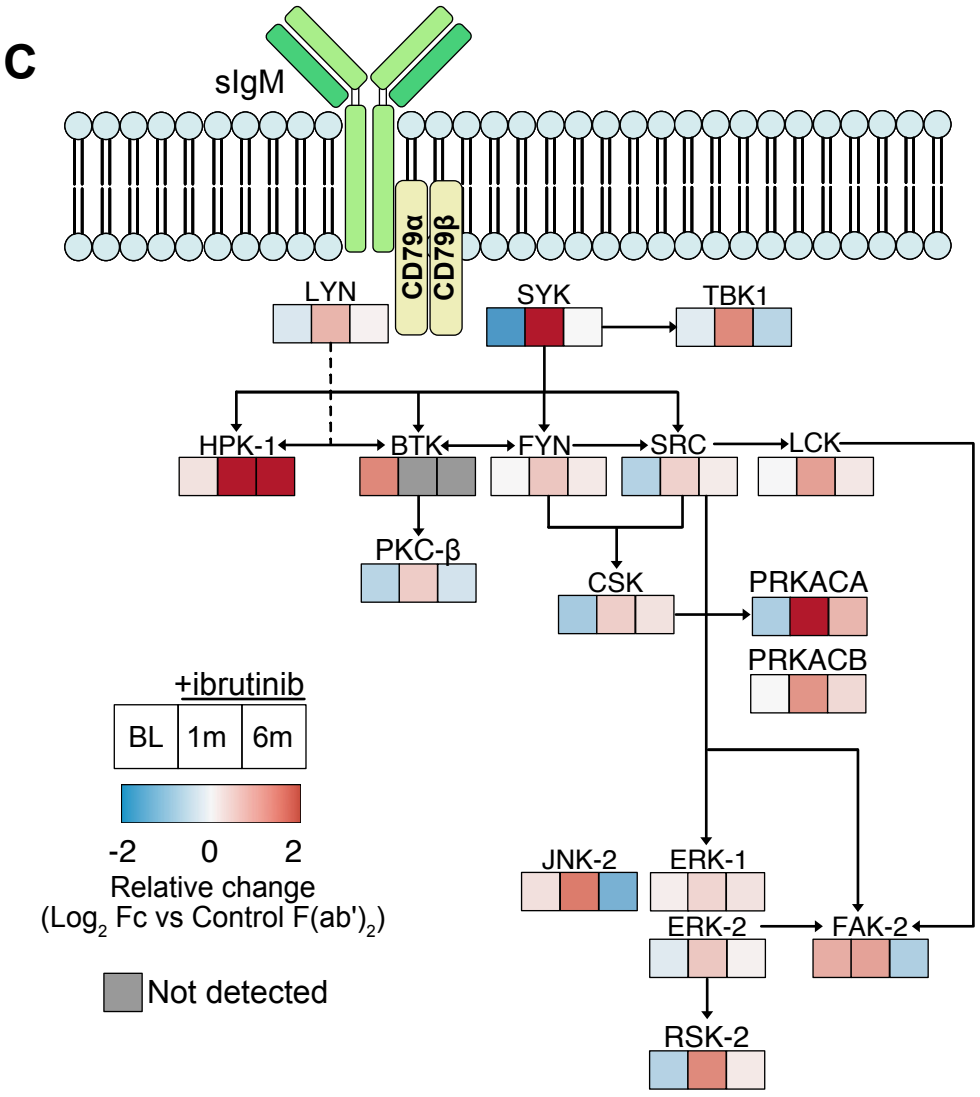

FIGURE 5